Combined Coarse-Grained and Atomistic Simulation of Liquid Bisphenol A−Polycarbonate: Liquid Packing and Intramolecular Structure

Cameron F. Abrams† and Kurt Kremer*

Max-Planck-Institut für Polymerforschung, Ackermannweg 10, 55128 Mainz, Germany

Received August 19, 2002

ABSTRACT: We present a new coarse-graining scheme for efficient molecular dynamics simulations of polycarbonate liquids and compare its effectiveness to that of a previously presented model which uses a different coarse-grained representation. The effect of more realistically accounting for the excluded volume of the phenylene comonomeric units in the coarse-grained simulation is examined. The new treatment avoids artifacts arising from sphere-packing, which dominate the liquid structure and dynamics in the older scheme, leading to a significant improvement in the equilibration time, for systems run at the typical processing temperature of 570 K. However, we observe only a slight improvement (10^{-4} eV/atom) in the equilibration of atomistically detailed samples that are inverse-mapped from the equilibrated coarse-grained configurations. Distributions in the atomistically resolved backbone bond and torsion angles are identical using the two schemes, as are computed liquid coherent scattering functions. This indicates that artifacts present at the coarsened level are effectively erased by equilibration at full-blown atomistic resolution, at least for systems with relatively short chains well above the glass transition temperature.

1. Introduction

Molecular coarse-graining has begun to play a larger role in simulation studies of polymers.[1−4] The chief aim in coarse-graining is to guarantee that the chain conformations in a simulation sample represent true equilibrium conformations. This requirement is effectively impossible to fulfill in direct atomistic simulations of polymer molecules, owing to limitations in computer power and characteristically long relaxation times for macromolecules. It is also fundamentally unfulfilled by "amorphous cell"-type atomistic simulations[5] designed to model glassy structure. A central feature of coarse-graining is that the models retain only as much unique and relevant information as needed about the specific polymer(s) under investigation, using significantly fewer degrees of freedom (i.e., particles) than required for full atomistic detail. The coarsened degrees of freedom must be constrained within ensembles of configurations which represent an appropriate average over the microscopic atomic-scale potential energy surface for the fully resolved system. Once an equilibrated sample at the coarse-grained level is generated using an appropriate simulation technique which samples these ensembles, atomic details can be inverse mapped to study atomic-scale properties and processes on appropriately short length and time scales.[6]

The choice of how one "maps" the atomic coordinates of a polymer onto a set of coarsened coordinates is of particular interest. The mapping points must be chosen such that intramolecular correlations at the coarsened level follow in a straightforward manner from averaging out atomic degrees of freedom over a postulated atomic-scale potential energy surface. Furthermore, for simulations of dense liquids, each mapping point must also play the role of a space-filling particle. They must therefore be chosen such that they as faithfully as possible mimic the true excluded volume "shape" of the molecule. The former requirement in general encourages larger degrees of coarsening, in which larger numbers of atomic degrees of freedom contribute to any one coarsened mapping point. The latter, on the other hand, supposes that any representation other than atomistic is nonoptimal. Hence, designing a mapping scheme is an optimization problem.

Recent work from our group presented a method for coarse graining melts of bisphenol A−polycarbonate (BPA−PC).[6−8] BPA−PC is by far the most utilized and intensively studied variety of polycarbonate, thanks to its many valuable material properties, such as high impact strength, ductility, and glass transition and melting temperatures.[9] For example, interesting questions regarding the mechanisms of glassy BPA−PC ductility have inspired many experimental,[10−15] simulation,[16−20] and combined experimental/simulation[21,22] studies, though remain essentially unresolved. Another interesting question is the origin of BPA−PC's surprisingly small entanglement molecular weight, M_e, of between six and seven chemical repeat units.[23] Understanding the origins of such unique properties would improve our ability to control these properties at the level of molecular design and synthesis. Simulations play a key role in gaining such understanding, providing means to systematically test hypotheses regarding the link between atomic scale structure and materials properties in well-characterized model systems. Coarse-grained simulations additionally give us, in principle, the ability construct model systems that behave properly on both the largest and smallest length scales relevant for such investigations.

In this article, we present an analysis of two different but otherwise valid choices for coarse-graining schemes of BPA−PC. Our intention is to show whether one or the other is better at producing an equilibrated atomic-scale liquid sample, and why. First, we briefly reintroduce the mapping scheme presented in ref 7, followed by a presentation of the newer scheme, in section 2. Our

† Present address: Department of Chemical Engineering, Drexel University, Philadelphia, PA 19104. E-mail: cfabrams@drexel.edu.

10.1021/ma0213495 CCC: $25.00
Published on Web 12/14/2002

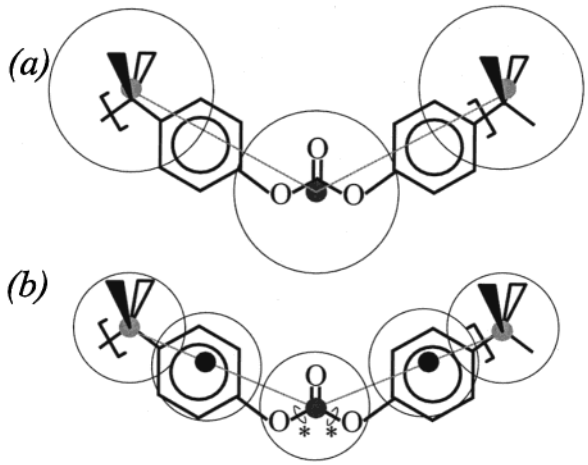

Figure 1. Schematic representations of the (a) 2:1 (ref 7) and (b) 4:1 mapping schemes for coarse-graining one repeat unit of BPA−PC. The large circles represent the approximate coarse-grained bead size relative to the atomic structure. The mapping points in the 2:1 scheme correspond to the centers of mass of the respective groups. Those in the 4:1 scheme correspond to the location of the respective backbone carbons. The additional beads in the 4:1 scheme correspond to the phenylenes only in that they represent the phenylene excluded volume more realistically than is done in the 2:1 scheme. "∗"'s denote the C_o-O torsions.

simulation and analysis techniques are then described in section 3, followed by results and discussion in section 4.

2. The Coarse-Grained Bead-Spring Models of BPA−PC

2.1. The 2.1 and 4:1 Mapping Schemes and Intermolecular Potentials. The general idea of coarse-graining is to represent a specific polymer molecule as a bead−spring chain. The role of the beads is 2-fold: first, they must, as a group, reflect the proper conformational statistics of the given polymer, and second, they must exclude volume such that the molecule fills space and has a "shape" as close as possible to the given polymer molecule. In the work presented here, all beads are spherical, and sphere−sphere (*ij*) excluded volume is ensured by a simple truncated and repulsive 12−6 Lennard-Jones pair potential with length parameter $\sigma_{ij} = {}^1/_2(\sigma_i + \sigma_j)$:

$$U_{\mathrm{LJ}}(r_{ij}) = \begin{cases} 4\epsilon\left[\left(\frac{\sigma_{ij}}{r_{ij}}\right)^{12} - \left(\frac{\sigma_{ij}}{r_{ij}}\right)^{6} + \frac{1}{4}\right] & r_{ij} < 2^{1/6} r_{ij} \\ 0 & r_{ij} \geq 2^{1/6}\sigma_{ij} \end{cases} \quad (1)$$

The choice of the σ_i's is explained in the following subsections. ϵ is chosen as the unit of energy, which we set at $k_B T$ for our *NVT* molecular dynamics simulations, discussed in section 3.

2.1.1. The 2:1 Mapping. A coarse-graining scheme for BPA−PC in which each repeat unit is replaced by two spherical beads connected by a harmonic spring was presented in ref 7. This "2:1" mapping scheme is shown schematically in Figure 1a. In this scheme, one bead corresponds to the position of the center of mass of an isopropylidene (−$C(CH_3)_2$−) subunit and the other to the center of mass of a carbonate (−O−CO−O−) subunit. The mapping points therefore do not exactly lie on the chain backbone. The positions of the linking phenylene groups are only implied by the relative positions of carbonates and isopropylidene, and the excluded volume of the phenylenes is represented partially by the excluded volume of neighboring the carbonate and isopropylidene, such that the total excluded volume of the repeat unit (measured as the sum of the volumes of the carbonate and isopropylidene beads) yields a bare total volume fraction in the liquid of 0.45 at a temperature of 570 K. In addition, smaller beads which represent the phenoxy chain ends are also included; this constitutes a slight modification over the previously presented 2:1 model,[7] where the specific structure of the chain ends was not taken into account. Note that the structure of a complete BPA−PC molecule has the formula C_6H_5−O−CO−O−(−C_6H_4−$C(CH_3)_2$−C_6H_4−O−CO−O−)$_n$−C_6H_5. As can be seen in ref 7, the ratio of bead diameter to average bond length is 1.24. This ratio has been shown to have a strong effect on the structure[24] and dynamics[25] of simple bead−spring liquids. To assess the effect of this commensurability artifact on the quality of the coarse-grained model, we developed a "4:1" mapping scheme, as discussed below.

Table 1. Lennard-Jones Scaling Parameter *S* and Coarse-Grained Bead Diameters (in Å) for the Two Coarse-Grained BPA−PC Mapping Schemes

scheme	S,Å/σ	σ_{Carb}, Å	σ_{Isop}, Å	σ_{Phen}, Å
2:1	5.56	5.29	5.84	2.74[a]
4:1	4.41	4.49	5.19	4.67

[a] Used for chain ends only.

Table 2. Harmonic Bond Potential Parameters for the Two Coarse-Graining Schemes: Mean Bond Length l_0 and Standard Deviation δl

scheme	Carb-Isop, Å	Carb-Phen, Å	Isop-Phen, Å
2:1	6.89 ± 0.07	3.61 ± 0.07[a]	−
4:1	-	3.56 ± 0.04	2.93 ± 0.04

[a] Used for chain ends only.

2.1.2. The 4:1 Mapping. In the newer 4:1 scheme, each repeat unit is still represented by two mapping points, corresponding respectively to the carbonate and isopropylidene subunits. In contrast to the 2:1 scheme, the mapping points are taken as the backbone carbons for each group rather than the group center of mass. Moreover, beads corresponding to the linking phenylene groups are included. The centers of these spheres do *not* correspond directly to the position of phenylene subunits, but are meant to only represent the groups' excluded volume in a more realistic way than in the 2:1 scheme. Each phenylene bead (except for the chain ends) is connected by stiff harmonic bonds to its neighboring isopropylidene and carbonate. The lengths of these bonds ensure the proper isopropylidene−carbonate intramolecular distance. Bond parameters, l_{ij} and δl_{ij}, and bead sizes, σ_i, for both schemes are given in Tables 1 and 2.

Bead sizes, σ_i, in the 4:1 model are computed by first calculating the gyration radii among atomic positions in each group, and then scaling these radii such that the volume of the repeat unit, accounting for the overlaps of adjacent beads, is equal to the van der Waals volume per repeat unit of BPA−PC computed using an equation-of-state analysis.[26] This yields a total volume fraction in the liquid of about 0.5. This is greater by about 10% compared to that in the 2:1 liquid; however, the *effective* excluded volume in the 2:1 system is at least 5−10% greater than the bare excluded volume due to the inaccessibility of the space immediately between

(nonoverlapping) adjacent beads along the chains. We therefore believe the volume fractions of the two coarse-grained models are close enough to allow comparison.

A subtle but important consideration requires this "loose" mapping to the phenylene group. Note that, given the atomic structure of the BPA−PC repeat unit, the angle formed by an isopropylidene backbone carbon, the phenylene center, and the carbonate carbon has a single value of about 167°. Tying a mapping point directly to the phenylene center also introduces a phenylene−isopropylidene−phenylene angle of about 109° and a phenylene−carbonate−phenylene angle defined by an appropriate distribution. However, because the angle around each phenylene is less than 180°, a torsional degree of freedom exists at each phenylene−carbonate bond. This torsional degree of freedom is correlated to the angle at the carbonate group. Without a complicated multibody potential, which must be a function of both a torsion and a bond angle, one cannot properly enforce this correlation. Rather than add to the complexity of the coarse-grained model in this way, we have opted to decouple the center of the phenylene bead with the center of the phenylene group in the atomic structure. Enforcing an angle of 180° at each phenylene bead excludes such torsional degrees of freedom, at the expense of not having *exact* knowledge of the location of any given phenylene group.

2.2. Intramolecular Potentials. Thus far we have discussed aspects of the bead excluded volume and bead−bead bond lengths for the two coarse-graining schemes. Further intramolecular constraints are used to ensure that the conformations which the chains sample reflect the proper statistics given the atomic-scale potential energy surface. As the details behind our technique were presented previously,[7] we present only a brief discussion here. These constraints take the form of bond angle and torsional potentials. For each carbonate−isopropylidene−carbonate ("c−i−c") and isopropylidene−carbonate−isopropylidene ("i−c−i") triple along a chain backbone, a potential, $U(\theta)$, is used which is a Boltzmann inversion of the corresponding probability density distribution for this type of angle, defined by the respective coarse-grained mapping points on the chain's atomic structure:

$$P(\theta) \propto \exp\left(-\frac{U(\theta)}{k_B T}\right) \tag{2}$$

The probability density distributions are computed via Monte Carlo sampling of the atomic structure of an isolated test chain. This sampling involved (1) random "moves" of backbone torsion angles $\{\phi\}$, (2) evaluation of the resulting total energy, and (3) acceptance based on a standard Metropolis criterion. The torsional energies, $\epsilon(\phi)$ were computed using Hartree−Fock calculations in the 6-31G* basis; details on these ab initio calculations appear in ref 7. Because the probability distribution P is tabulated as a histogram, but is a function of polar angle, we normalize by the appropriate volume element when extracting the force:

$$f(\theta) = -\frac{\partial}{\partial\theta}\left[\ln\left(\frac{P(\theta)}{\sin\theta}\right)\right] \tag{3}$$

Tabulated forces were computed via second order finite differences.

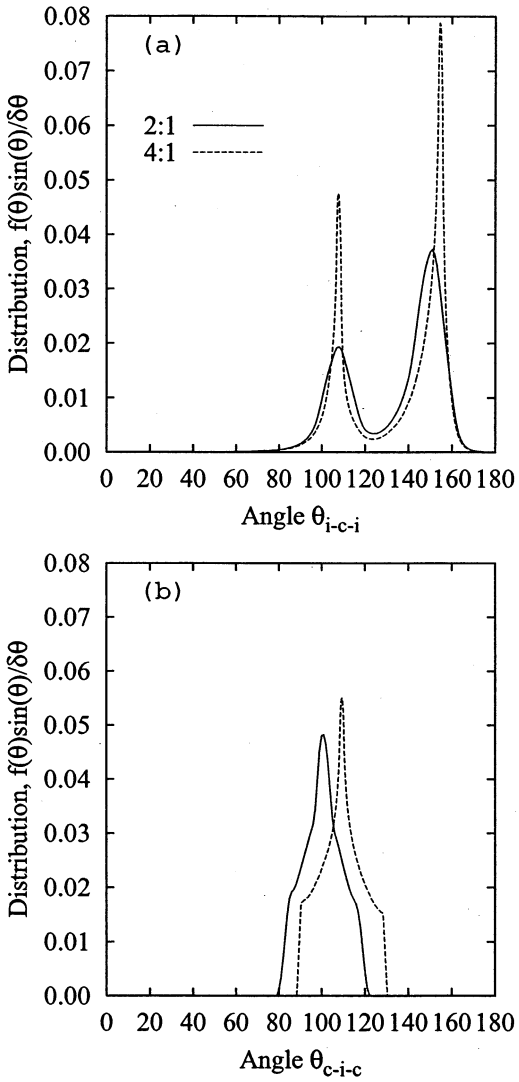

Figure 2. Probability distribution functions for coarse-grained bond angle at (a) the carbonate group, and (b) the isopropylidene group for the 2:1 (solid) and 4:1 (dashed) mapping schemes. The functions are presented in histogram form; $\delta\theta$ is the bin size.

Density distributions P for the i−c−i and c−i−c angles are shown in Figure 2 for both coarse-graining schemes. The differences arise only due to the different choices for the mapping points: in the 4:1 scheme, mapping points lie exactly on their respective backbone atoms, while in the 2:1 scheme, these points correspond to comonomer centers of mass. Because these centers of mass do not lie on the backbone, they can sweep a larger volume of space than points that lie directly on the backbone. Hence, the 2:1 distributions are generally broader. The peak in the c−i−c distribution is located at a lower angle because the center of mass of the isopropylidene comonomer lies within the triangle formed by the backbone carbon and the two dangling methyl carbons, which is always further from the neighboring carbonates than the backbone carbon. This 2:1 isopropylidene mapping point thus forms a more acute average bond angle than that in the 4:1 model, which lies directly on the backbone carbon.

Furthermore, i−c−i−c torsional potentials are also applied in the case of the 2:1 model, although the torsional barrier introduced by this potential at 570 K is only about 0.1 $k_B T$.[7] In the case of the 4:1 model, these

are ignored completely because the torsional barrier introduced by this potential is much less than 0.1 k_BT at 570 K. Short test calculations in which these torsional potentials were explicitly included yielded statistically identical results. For studies at lower temperatures the inclusion of a torsional barrier might however become relevant again.

The structure of $P(\theta_{i-c-i})$ in both the 2:1 and 4:1 models is of particular interest, because it reveals the "two-state" nature of the carbonate bond angle in coarse-grained BPA−PC. The lower peak corresponds to cis−trans conformations of the two C_o−O torsions in the carbonate group, (denoted with "∗" in Figure 1b) and the larger peak to trans−trans conformations, which are energetically more favorable. The distributions shown in Figure 2 demonstrate that both states are populated at $T = 570$ K, with roughly $^2/_3$ of carbonates in the trans−trans conformation.

In the 4:1 model, backbone bond angles at the phenylene beads are enforced at 180° by a simple harmonic potential with a spring constant of 0.1 k_BT/deg^2. Because phenylenes that are immediate neighbors on either side of the same isopropylidene bead can weakly overlap, the excluded volume interaction for these intramolecular phenylene−phenylene pairs is turned off. This choice has a measurable effect on the resulting bond angle distributions around the isopropylidenes, and it was observed that leaving this interaction in place strongly compromises the ability of the "c−i−c" Boltzmann-inverted potential to enforce the expected bond angle "c−i−c" distribution. However, as we shall see in section 4.1, leaving this interaction out of the model does not fully correct this problem.

3. Molecular Dynamics Simulation Description

3.1. Coarse-Grained Samples. Molecular dynamics simulation was used to equilibrate samples of coarse-grained bead−spring chains prior to the introduction of atomic scale details. The simulations performed for this study are formally identical to those of ref 7. Here we provide a brief discussion. The potentials used in the simulation were discussed in the previous section. The velocity−Verlet algorithm was used to integrate the particle equations of motion using a constant time step of 0.01 τ. A Langevin-type thermostat with friction $\Gamma = 0.5\ \tau^{-1}$ was used to keep the temperature constant at 1.0. Reduced Lennard-Jones units were used throughout, where the length conversion factor S was 5.56 Å/σ in the 2:1 system and 4.41 Å/σ in the 4:1 system. These values of S were originally chosen such that the desired volume fraction of the liquid system, about 0.45, is given[7] at a number density of 0.85/σ^3; however, due to the addition of chain ends in the modified 2:1 scheme, this is strictly only true for the 4:1 system. Energy is measured in units of k_BT for $T = 570$ K, the temperature at which the Boltzmann averaging of the atomic structure to give the coarse-grained distribution functions is performed.

The liquid samples were generated by first specifying a number of chains and number of repeat units per chain and the system density. Chains were then randomly placed in a box and grown according to the bond length and bond angle probability constraints; for details, see ref 7. To remove bead−bead overlaps, the raw systems are run using the following bead−bead Lennard-Jones potential:

$$U_{\text{warmup}}(r_{ij}) = \begin{cases} 4\epsilon\left[\left(\dfrac{\sigma_{ij}}{r_{ij}+2^{1/6}\sigma_{ij}b(t)}\right)^{12} - \left(\dfrac{\sigma_{ij}}{r_{ij}+2^{1/6}\sigma_{ij}b(t)}\right)^{6} + \dfrac{1}{4}\right] & [r_{ij} + 2^{1/6}\sigma_{ij}b(t)] < 2^{1/6}\sigma_{ij} \\ 0 & [r_{ij} + 2^{1/6}\sigma_{ij}b(t)] \geq 2^{1/6}\sigma_{ij} \end{cases} \quad (4)$$

where the factor $b(t)$ decays linearly from unity to zero over the duration of the warmup stage:

$$b(t) = \frac{t_f - t}{t_f - t_i}$$

Here, t_i and t_f are the initial and final time values of the warmup stage, respectively.

All samples consisted of 80 chains of 10 repeat units each. This corresponds to chains of 23 beads in the 2:1 scheme and 43 beads in the 4:1 scheme. The system density was fixed at 1.05 g/cm^3, the experimental system density at 570 K. Since we fix the mass density, this results (for $N = 10$) in a particle number density of 0.91/σ^3 in the 2:1 system and 0.85/σ^3 in the 4:1 system. The resulting cubic box was 70.28 Å on a side.

One can see that it requires roughly twice as many particles to represent a particular system in the 4:1 mapping scheme as in the 2:1 mapping scheme. In general, the computational effort in calculation of pairwise forces in a particle simulation scales with the square of the number of particles. This seemingly implies that four times as many CPU cycles are required to simulate a 4:1 system for a given amount of integration time, compared to a 2:1 system. This is not the case in our simulation program, which uses the "link-cell" algorithm[27] in the computation of pairwise forces. This algorithm scales linearly with the number of particles, so only twice as many CPU cycles are required to simulate the 4:1 system. If the time to equilibrate 4:1 chains is less than half the time required to equilibrate 2:1 chains, then the 4:1 scheme is more efficient than the 2:1 scheme. This will be addressed in section 4.1.

After the warmup phase, each system was integrated for an adequate amount of time to equilibrate the chains in the melt. As a working definition, equilibration was achieved when the mean squared displacement of chain centers of mass exceeds the chain mean squared radius of gyration. This equilibration time, τ_{eq}, for each run is reported in Table 3.

Table 3. Summary of Results from the $N = 10$ Coarse-Grained Simulations

scheme	P, MPa	ζ, τ^{-1}	t_{eq}, τ	$\langle R_g^2/N\rangle$, Å^2
2:1	2000.	1400.	50000.	36.4
4:1	640.	70.	6000.	37.3

3.2. Inverse Mapping. Only after equilibration of the coarse-grained systems can we safely introduce atomic details, confident that the system is equilibrated on the scale of entire chains. The inverse mapping procedure used in this work is identical to that discussed in detail in ref 6. Briefly, for each coarse-grained chain, an atomistic chain was created. While keeping the coordinates of the beads in the coarse-grained chain fixed, the torsion angles $\{\phi\}$ and Euler angles (α,β,γ) of the atomic chain were varied according to a conjugate gradient minimization of least squares, where the error was the sum of distances from the coarse-grained beads to the appropriate mapping points on the atomic chains. Errors were minimized to better than 10^{-2} Å. This procedure was done for each chain independently, with no energy evaluation.

3.3. Atomistically Resolved Samples. Once the inverse mapping has been performed, atomistic MD is performed using the Yasp simulation package.[28] The first step is the generation of a molecular topology description. The molecular mechanics force-field parameters used for BPA−PC were reported previously;[29] these are used in this work without modification, and for the sake of brevity we do not report them here. These parameters define bond constraints and intramolecular potentials which include harmonic bond angles and dihedrals, torsions, and intermolecular potentials that include standard Lennard-Jones and reaction-field-modified electrostatics. Each atomistic sample of 80 chains of 10 repeat units each consists of total of 28 480 atoms. The first phase of the atomic scale equilibration is another warmup to remove atomic-scale overlaps. This requires three sequential 10 ps integrations using a "soft core" intermolecular potential instead of the Lennard-Jones plus electrostatics. The soft core potential linearly decreases from some specified value A at a distance

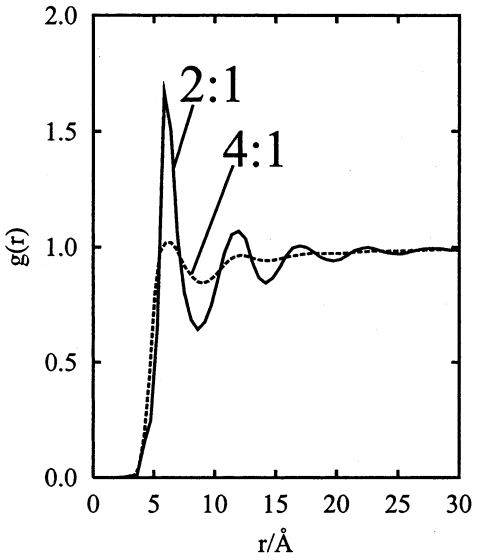

Figure 3. Radial distribution functions, $g(r)$, from the coarse-grained simulations.

of 0 to zero at a specified distance r_{sc} for all pairs of atoms in the system. The values of A in these three runs were 50, 100, and 150 kJ/mol, and r_{sc} is 3.98 Å. As with the coarse-grained simulations, the standard velocity−Verlet integrator was used, here with a time step of 0.001 ps. The temperature was set at 570 K and controlled using a Berendsen-type thermostat with a coupling constant of 0.2 ps. After the final warmup, the full Lennard-Jones and electrostatic potentials were used, and a 5 ps integration with a time step of 0.0005 ps was performed. The final step was a production run of 300 ps with a time step of 0.001 ps.

4. Results and Discussion

4.1. Liquid Structure and Dynamics at the Coarse-Grained Scale. To begin understanding the differences in the two mapping schemes, we present radial distribution functions of the coarse-grained liquids in Figure 3. These $g(r)$s reveal a strong distinction between the two schemes, namely, that beads in the 2:1 scheme can pack more efficiently than beads in the 4:1 scheme, as evidenced by the stronger nearest-neighbor and second-nearest-neighbor peaks. This is because the backbone bonds are long enough such that they do not disrupt the natural packing length for a liquid of dense spheres with sizes given by the 2:1 scheme. This commensurability is expressed as a ratio of mean bond length to bead diameter, l/d, and for dense systems (volume fractions greater than about 0.4) the strongest effects of commensurability are observed for $l/d > 1$.[24] As discussed previously, l/d in the 2:1 scheme is 1.24, whereas in the 4:1 scheme, l/d ranges between 0.7 and 0.8. This allows the spherical beads in the 2:1 system to pack in much the same manner as do spheres in a simple monomeric liquid at the same volume fraction. One result of this packing is a higher pressure in the 2:1 system, as shown in Table 3. (Note that because we have included no long-range attractions in the coarse-grained system, this pressure simply reflects bead−bead excluded volume within the cutoff radius of the potential, which is $2^{1/6}\sigma_{ij}$ for beads i and j.)

Another important consequence of this more efficient sphere-packing has to do with the ability of the intramolecular potentials to enforce the proper bond angle statistics. If we consider, for illustrative purposes, a freely jointed chain melt with an l/d of 1.24, we find that

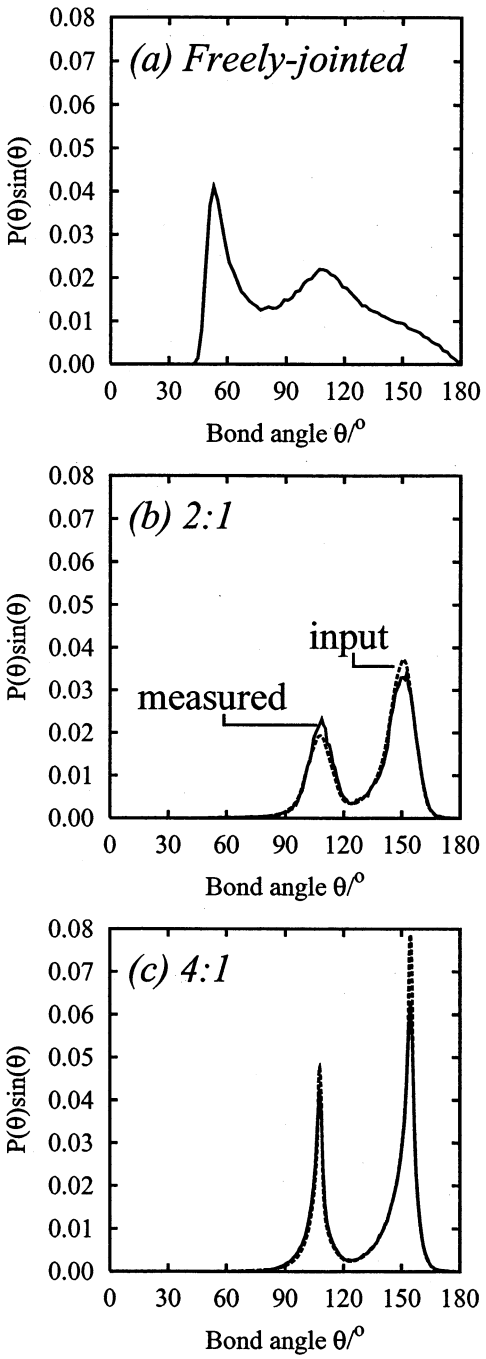

Figure 4. Bond angle distributions, $P(\theta)$, in bead−spring liquids: (a) for freely jointed chains; (b) around carbonate groups (P_{carb}) in 2:1 coarse-grained BPA−PC, showing the input (dashed) distribution and the distribution measured from MD simulation (solid); (c) for the same as part b but for 4:1 BPA−PC.

the packing in the liquid induces structure in the bond angle distributions $P(\theta)$ for the chains. This is depicted in Figure 4a. Note that structure in $P(\theta)$ appears to arise naturally due solely to preferred relative orientations of triples of spheres packed in a dense liquid. The major peak at 60° occurs when the next-nearest-neighbors in the triple sense each other via the excluded volume interaction, and the second peak at ≈120° corresponds to a single external bead between these two.

This naturally arising structure in P influences the measured P for carbonate groups (P_{carb}) in the case of the coarse-grained 2:1 BPA−PC. The strong peak in P_{carb} at $\theta \approx 115°$ enhances the first peak of P_{carb} for 2:1

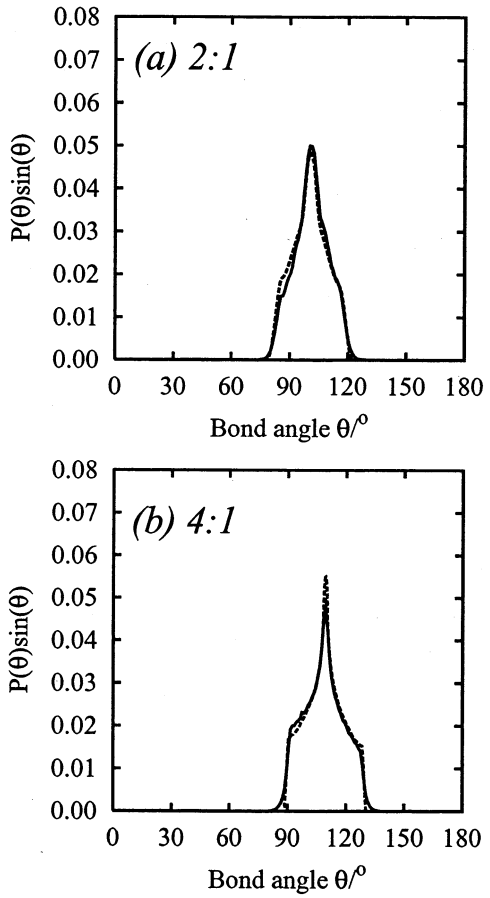

Figure 5. Bond angle distributions around isopropylidene groups, P_{iso}, in (a) the 2:1 and (b) the 4:1 model simulations, showing the input (dashed) distribution and the distribution measured from MD simulation (solid).

BPA−PC, overpopulating this state in P_{carb} relative to the input distribution by about 5%. This corruption of the chain statistics at the carbonate angles is observed to be much weaker in the 4:1 scheme (Figure 4c), because the bond lengths are too short to be commensurate with sphere-packing, as evidenced by the weaker peaks in $g(r)$ relative to the 2:1 scheme. The major effect realized in the measured bond angle distributions in the 4:1 scheme is a slight broadening of the cis−trans peak toward lower bond angles. This is most likely a weaker manifestation of the same mechanism.

Similar effects can be seen in comparing the input and measured distributions around the isopropylidenes (P_{iso}) in both mapping schemes. In Figure 5a, we show the input and measured P_{iso} for the 2:1 mapping scheme. This shows a slight preference for more open bond c−i−c bond angles in the dense liquid relative to the input distribution. This cannot be due to next-nearest-neighbor carbonate−carbonate excluded volume, because this would only prevent angles of less than about 45° around the isopropylidenes. Instead, this is likely due again to the preference for angles which are allowed due to dense sphere packing, which in this case would select for angles greater than the average of about 100°, because c−i−c angles of less than about 80° are excluded. In the 4:1 model, we observe an opposite effect. The measured P_{iso} shows a slight preference for more acute bond angles. This is indeed due to (1) the *lack* of next-nearest-neighbor phenylene−phenylene excluded volume and (2) the smaller size of the carbonate beads,

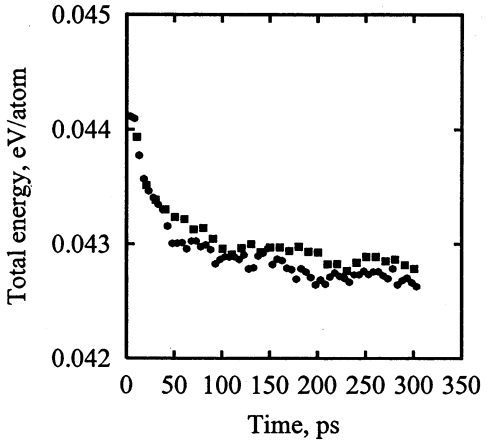

Figure 6. Total energy per atom vs integration time for the atomic-scale MD simulations. The atomistic system inverse mapped from the 2:1 coarse-grained system (squares) is compared to that of the 4:1 coarse-grained system (circles).

relative to the 4:1 model. It should be emphasized that all of these effects are indeed quite small relative to the overall measures of chain statistics. Indeed, the measured root-mean-squared radii of gyration per repeat unit are essentially the same for the two models, as shown in Table 3. Large distinctions in artifacts in the measured bond angle distributions would be expected to show up as large differences in measured $\langle R_g^2 \rangle^{1/2}$, which we do not observe.

A preliminary comparison of the dynamic behavior of the two models was presented previously.[30] There it was shown that the 2:1 model suffered from much larger bead frictions ζ in the liquid compared to the 4:1 model, and that this arose clearly from the commensurability of bond length and bead diameter.[25] The conclusion was that the 4:1 model, though it requires tracking double the number of particles as the 2:1 model for chains of the same number of repeat units, results in significantly shorter run times to produce equilibrated chains. These results are included as ζ and equilibration times τ_{eq} in Table 3. We see from Table 3 that 4:1 chains equilibrate almost nine times faster than 2:1 chains, yielding an effective speed up factor of 4.5 compared to the 2:1 scheme.

4.2. Intramolecular Statistics and Energetics at the Atomic Scale. The 300 ps MD integration of the atomic coordinates after remapping and warming serves to equilibrate the atomic system on short length scales. This means that at the length scale of entire chains, very little rearrangement occurs. A possible consequence is that any artifacts introduced due to the nature of the coarse-grained model are likely to survive at the atomistic level. In this section, we discuss why this is not the case.

In Figure 6, we show the trace of total energy vs time for the two atomistic trajectories. We see that this energy decays to a steady value after about 100 ps and that the total energy in the 4:1 inverse mapped system is slightly lower. However, this difference amounts to about 10^{-4} eV/atom, about 1.1 K, which is practically insignificant.

This close agreement in total energy is mirrored by the close agreement in chain statistics. As examples, we show the measured distributions of torsion angles at the bonds between bridging oxygens and carbonate carbon atoms (denoted "*" in Figure 1b) in Figure 7. These torsional degrees of freedom are responsible for

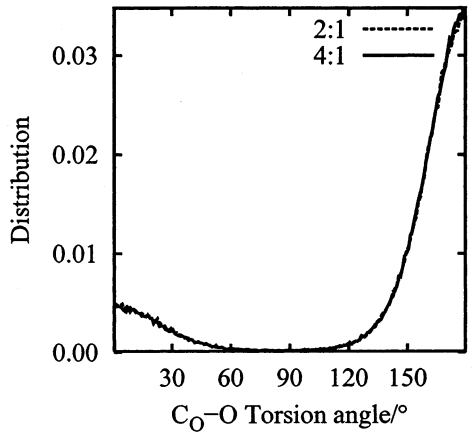

Figure 7. Distributions in the C_o–O torsion angles averaged over the final 100 ps of the atomistic simulation trajectories. The atomistic system inverse mapped from the 2:1 coarse-grained system (dashed) is compared to that of the 4:1 coarse-grained system (solid).

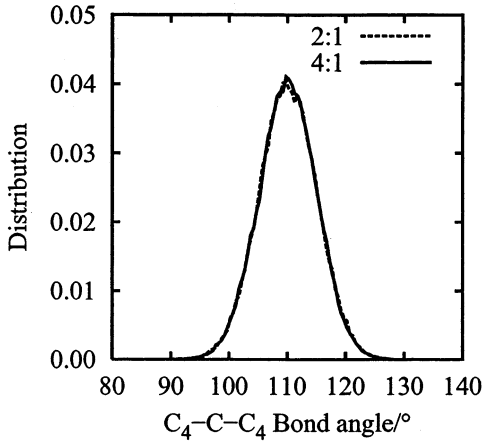

Figure 8. Distributions in the backbone C_4–C_{iso}–C_4 angles averaged over the final 100 ps of the atomistic simulation trajectories. The atomistic system inverse mapped from the 2:1 coarse-grained system (dashed) is compared to that of the 4:1 coarse-grained system (solid).

most of the configurational freedom of BPA–PC molecules. As shown in the figure, distributions arising from 2:1 coarsened systems are essentially identical to those arising from 4:1 systems. This is similarly reflected in the distributions of backbone bond angles at the isopropylidene carbon atoms, shown in Figure 8. It is therefore clear that the intramolecular atomic structures predicted by both schemes are, for statistical purposes, identical at the present temperature.

Intermolecular liquid structure in the atomically resolved systems are easily assessed by means of the coherent scattering function,

$$S(q) = \sum_{ij} \langle b_i \rangle \langle b_j \rangle \exp(i\mathbf{q}\cdot(\mathbf{r}_i - \mathbf{r}_j)) \qquad (5)$$

The scattering lengths used here are those reported in ref 31: $b_H = -3.741 \times 10^{-4}$ cm, $b_O = 0.6674 \times 10^{-4}$ cm, and $b_C = 0.6648 \times 10^{-4}$ cm. $S(q)$ is computed for wave vectors $\mathbf{q}$ whose components are integer multiples of $2\pi/L$, where L is the box size. We computed $S(q)$ over 100 sequential configurations, each separated by 1 ps in MD integration time. $S(q)$ for the 2:1 and 4:1 systems are shown in Figure 9. Included in Figure 9 is also $S(q)$ for a solid sample of BPA–PC determined by spin-

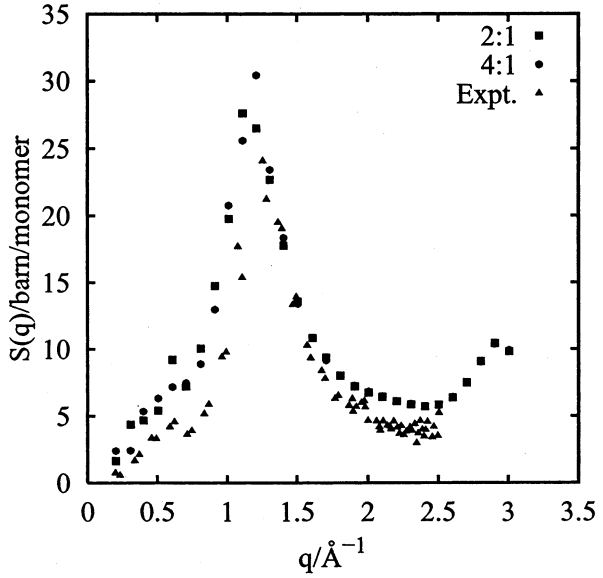

Figure 9. Coherent scattering functions, $S(q)$, averaged over 100 snapshots at 1 ps intervals over the final 100 ps of the atomistic simulation trajectories. The atomistic system inverse mapped from the 2:1 coarse-grained system (squares) is compared to that of the 4:1 coarse-grained system (circles); also included are experimental results for solid BPA–PC (triangles) (Modified from ref 31).

polarized neutron scattering, which is taken from a previous paper.[31]

The scattering functions demonstrate that the atomic structure of the liquids generated using the two coarse-graining schemes are essentially identical. Moreover, both do a surprisingly good job reproducing the experimentally determined $S(q)$, considering that the latter is measured on a solid sample of BPA–PC at 4 K, which has a density roughly 15% higher than the liquid. For wavevectors greater than 1.5 Å^{-1}, corresponding to length scales less than $2\pi/1.5 = 4.2$ Å, the two simulated $S(q)$'s are numerically identical, which is not surprising given that this probes atomic structure on length scales less than about one repeat unit. For the smaller wavevectors ($q < 1.5$ Å), the differences in the two computed $S(q)$'s do not appear to be systematic, and most likely arise from density fluctuations which are longer-lived than the sampling time. In light of the comparison to experiment, however, the conclusion that both mapping schemes produce accurate atomically resolved liquids is further confirmed.

5. Conclusions

We have discussed two coarse-graining simulation schemes for producing equilibrated liquid samples of 10 repeat unit bisphenol A–polycarbonate with full atomistic resolution. The two-step procedure for producing the atomically resolved samples involved MD simulation of the coarsened chains and then reintroduction of the atomistic details followed by a full-blown atomistic simulation. The chief difference between these two schemes is in how the excluded volume of the phenylene comonomers is treated: in the newer, 4:1 scheme, this excluded volume is assigned to a distinct spherical particle, rather than partitioned into the excluded volume of the carbonate and isopropylidene comonomer particles, as was done in the 2:1 scheme.[7] We show that the newer 4:1 coarse-grained model does a slightly better job producing an equilibrated atomic scale sample,

as measured by the total energy per atom after 300 ps MD integrations. Statistical measures of chain atomic structures were essentially identical for both cases, as were bulk structure factors, indicating that both schemes yield the same atomic structure in the liquid. The most important result of this work is in demonstrating that potentially harmful artifacts introduced by simplifications in the coarse-grained model can be effectively nullified via straightforward MD integration at full atomistic resolution. We suspect that this fortunate circumstance is related to the physical conditions chosen for the simulations, i.e., a temperature well above the glass transition and a corresponding density somewhat lower than in the glassy state, though at the actual experimental melt density at $T = 570$ K. It is therefore of extreme interest to examine how sensitively coarse-grained artifacts are communicated to systems of atomistic resolution for glassy systems. Nevertheless, the current work provides powerful testimony to the usefulness and potential success in further development of such coarse-graining techniques.

Acknowledgment. This work was supported by the Germany Ministry of Education and Research, under Grant No. 03 N 6015, and the Bayer Corp. We thank F. Bruder, L. Delle Site, and F. Müller-Plathe for useful discussions.

References and Notes

(1) Baschnagel, J.; Binder, K.; Doruker, P.; Gusev, A. A.; Hahn, O.; Kremer, K.; Mattice, W. L.; Müller-Plathe, F.; Murat, M.; Paul, W.; Santos, S.; Suter, U. W.; Tries, V. *Adv. Polym. Sci.* **2000**, *152*, 41−156.
(2) Paul, W.; Binder, K.; Kremer, K.; Heermann, D. W. *Macromolecules* **1991**, *24*, 6332−6334.
(3) Kremer, K.; Müller-Plathe, F. *MRS Bull.* **2001**, *26*, 205−210.
(4) Müller-Plathe, F. *ChemPhysChem.* **2002**, *3*, 754−769.
(5) Theodorou, D. N.; Suter, U. W. *Macromolecules* **1985**, *18*, 1467−1478.
(6) Tschöp, W.; Kremer, K.; Hahn, O.; Batoulis, J.; Bürger, T. *Acta Polym.* **1998**, *49*, 75−79.
(7) Tschöp, W.; Kremer, K.; Batoulis, J.; Bürger, T.; Hahn, O. *Acta Polym.* **1998**, *49*, 61−74.
(8) Hahn, O.; DelleSite, L.; Kremer, K. *Macromol. Theor. Simul.* **2001**, *10*, 288−303.
(9) Morbitzer, L.; Grigo, U. *Angew. Makromol. Chem.* **1988**, *162*, 87−107.
(10) Yee, A. F.; Smith, S. A. *Macromolecules* **1981**, *14*, 54−64.
(11) Schaefer, D.; Hansen, M.; Blümich, B.; Spiess, H. W. *J. Non-Cryst. Solids* **1991**, *131−133*, 777−780.
(12) Floudas, G.; Higgins, J. S.; Meier, G.; Kremer, F.; Fischer, E. W. *Macromolecules* **1993**, *26*, 1676−1682.
(13) Weigand, F.; Spiess, H. W. *Macromolecules* **1995**, *28*, 6361−6384.
(14) Wimberger-Friedl, R.; Schoo, H. F. M. *Macromolecules* **1996**, *29*, 8871−8874.
(15) Li, L.; Yee, A. F. *Macromolecules* **2002**, *35*, 425−332.
(16) Shih, J. H.; Chen, C. L. *Macromolecules* **1995**, *28*, 4509−4515.
(17) Fan, C. F.; Tahir, C.; Shi, W. *Macromol. Theory Simul.* **1997**, *6*, 83−102.
(18) Tsai, S. F.; Lan, I. K.; Chen, C. L. *Comp. Theor. Polym. Sci.* **1998**, *8*, 283−289.
(19) Bendler, J. T. *Comp. Theor. Polym. Sci.* **1998**, *8*, 83−92.
(20) Ballone, P.; Montanari, B.; Jones, R. O.; Hahn, O. *J. Phys. Chem. A* **1999**, *103*, 5387−5398.
(21) Robyr, P.; Gan, Z.; Suter, U. W. *Macromolecules* **1998**, *31*, 6199−6205.
(22) Utz, M.; Robyr, P.; Suter, U. W. *Macromolecules* **2000**, *33*, 6808−6814.
(23) Fetters, L. J.; Lohse, D. J.; Milner, S. T.; Graessley, W. W. *Macromolecules* **1999**, *32*, 6847−6851.
(24) Abrams, C. F.; Kremer, K. *J. Chem. Phys.* **2001**, *115*, 2776−2785.
(25) Abrams, C. F.; Kremer, K. *J. Chem. Phys.* **2002**, *116*, 3162−3165.
(26) Sanchez, I. C.; Cho, J. *Polymer* **1995**, *36*, 2929−2939.
(27) Frenkel, D.; Smit, B. *Understanding Molecular Simulation: From Algorithms to Applications*, 2nd ed. Academic Press: San Diego, CA, 2002.
(28) Müller-Plathe, F. *Comput. Phys. Commun.* **1993**, *78*, 77−94.
(29) Hahn, O.; Mooney, D. A.; Müller-Plathe, F.; Kremer, K. *J. Chem. Phys.* **1999**, *111*, 6061−6068.
(30) Abrams, C. F.; Kremer, K., in *Proceedings of CIMTEC 2002−10th International Ceramics Conference & third Forum on New Materials, Florence, Italy*; Vincenzini, P., Ed.; Techna Publishers, S.r.l.: Italy, 2002.
(31) Eilhard, J.; Zirkel, A.; Tschöp, W.; Hahn, O.; Kremer, K.; Schärpf, O.; Richter, D.; Buchenau, U. *J. Chem. Phys.* **1999**, *110*, 1819−1830.

MA0213495